V. L. Rvachev

T. I. Sheiko

Institute for Problems in Machinery,
Academy of Sciences of Ukraine,
Kharkov, Ukraine

V. Shapiro

J. J. Uicker

Mechanical Engineering Department,
University of Wisconsin-Madison,
Madison, WI

Implicit Function Modeling of Solidification in Metal Castings

Solidification of metal castings can be modeled by an implicit real-valued function whose behavior is determined by physical parameters prescribed on the boundary of a casting. We show how to construct such functions using theory of R-functions for two-dimensional castings represented by their boundaries. The parameterized form of the constructed functions is convenient for studying, controlling, and optimizing their behavior in terms of the physical parameters specified on the boundary of the casting. The proposed approach can also be used for modeling multiple cavities in a same sand mold, generalizes to three-dimensional castings, and is applicable to other physical phenomena that may be suitable for analysis based on empirical knowledge.

1 Introduction

1.1 Physical Aspects of the Casting Process. After being delivered into the casting cavity molten metal assumes the configuration of the latter and proceeds to cool. Upon reaching the liquidus temperature the alloy starts to solidify. Solidification rate characterizes the increasing volume of the solid phase with time and depends on the heat transfer rate. The outer shell skin of the mold forms during this time, displaying a tendency towards chemical heterogeneity, development of casting shrinkage as well as surface layer formation. Upon completion of cooling the casting should have a uniform density and homogeneity, minimal internal stress and a smooth and clean surface. All these requirements can only be fulfilled by the correct use of the laws that define the casting solidification process and various defect prevention measures.

Sand and thin-wall metallic 3D custom castings are quite distinct in terms of their thermophysical properties. The mold in a sand cast heats at a low rate, as the thermal conductivity is high compared to the heat transfer coefficient. However, the cooling rate of the casting itself is higher as its thermoconductivity is low compared to the heat transfer coefficient because of the considerable thickness and the low heat conductivity of the material. We can consider a 3D sand mold to be semi-infinite as its outer surface does not heat up noticeably during solidification of the casting. It is known (Mikhailov et al, 1987) that the thickness of the solidifying layer at the casting surface is proportional, and the linear rate of thickness frozen is inversely proportional to $\sqrt{t}$ when cooling in a sand mold. The linear rate of solidification of the casting drops with time, i.e. the rate is not the same along the section of the mold and is substantially lower in the central zone of a planar mold. Complex form castings used to be viewed as consisting of planar, cylindrical and spherical parts with their relative size values $L = V/F$, where V is volume and F is the surface area of the casting. In cylindrical and spherical castings, as opposed to planar ones, the linear rate of solidification does not drop by the end of the process, but increases due to the change in the ratio of the solidifying metal volume to the cooling surface. The regularities of mold solidification in 3D sand casts are applicable to other types of casts. Only in the case of using thin-wall water-cooled metal casts (without coating) for making thin-walled castings the thickness of solidifying metal layer does change linearly with time, and the solidification rate becomes constant.

Contributed by the Design Automation Committee for publication in the JOURNAL of MECHANICAL DESIGN. Manuscript received Dec. 1996; revised July 1997. Associate Technical Editor: B. Ravani.

The pouring-feeding systems, i.e. the systems of channels and rigging elements of the cast, are used for the delivery of metal and filling of the cast cavity, as well as feeding of the mold during solidification. The choice of metal delivery and regulation of its flow during filling of the form can create a desired regime of solidification and allow manipulation of the structure and physical properties of the casting to a certain extent. With the use of the pouring-feeding system the mode of solidification and cooling of the mold can be regulated, thus creating directional solidification. For this purpose external and internal coolers can be used.

Complexity of the physical process and geometric information makes mathematical modeling of solidification difficult and computationally intensive. In this paper we show that many of these difficulties can be overcome through implicit function models constructed using theory of R-functions.

1.2 Postulated Mathematical Properties. Mathematical models of physical processes should be consistent with available experimental data and known physical laws. Such information and engineering intuition suggests that the following set of postulates form a reasonable basis for mathematical modeling of metal casting:

(1) If the initial temperature is constant along the boundaries of the form, the solidification of metal will take place along the points that are equidistant from the initial boundaries. In particular, if the initial boundaries are linear, then the transition between the solid and liquid metal remains linear.

(2) Experimentally validated Chvorinov's rule (Chvorinov, 1940) states that

$$\log t = k \log (V/A) + b,$$

where V is a total casting volume, A is a total surface area, t is a total solidification time, and b, k are constants.

(3) The speed of metal solidification, and therefore the location of unsolidified metal, depends on prescribed heating or cooling conditions at the boundary portions of the original form and its interaction with adjacent forms, insulators, and chills (if present). This gives a method for moving and eliminating defects associated with the final stages of solidification.

(4) Except in the final stages of solidification (that could be followed by shrinkage), the physical nature of the solidification process suggests no discontinuities in the

temperature field, temperature fluxes, and the resulting stress fields.

(5) Sharp corners in the mold affect the speed of the solidification. In particular, for two-dimensional forms it has been established (Neises et al., 1987) that in the vicinity of a convex right angle the isothermal lines are determined by

$$\frac{xy}{x+y} = \text{const},$$

where x and y are distances to the edges forming the right angle. More generally, the solidification process speeds up near the convex angles and slows down in the vicinity of the reflex angles.

(6) The ambient temperature remains constant at all points that are sufficiently far from the mold and will be called the "temperature at infinity."

1.3 Choice of Mathematical Models. A common empirical method for predicting solidification of metal in castings relies on a "inscribed rolling ball" analogy. The center of a ball rolling along the smooth boundary of the casting gives the set of points that are equidistant from the boundary and therefore can be used as a heuristic measure of the solidification speed. Another way to describe equidistant points is by level contours of so called normal function f of the boundary (Rvachev, 1967, 1982; Kutsenko, 1990; Kutsenko and Markin, 1994). The equation of the boundary $\Gamma = (f = 0)$ is called normal if the value of $f(p)$ is equal to the Euclidean distance from point p to the boundary Γ. Similarly a function f that coincides with the normal function only on the boundary Γ is called normalized and has a property that $(\partial f/\partial \nu)|_\Gamma = 1$.

In this paper we show how normal and normalized functions can be used for modeling solidification in metal castings. Constructing such functions for reasonably complex castings requires a general mathematical method to transform geometric information (such as boundaries of the mold) into an analytic model (in this case, an implicit function). The methods for constructing the needed implicit function used in this paper are based on the theory of R-functions (Rvachev, 1967, 1982; Shapiro, 1988) which is briefly introduced below.

2 Construction of Implicit Functions

2.1 Method of R-Functions. Function $y = f(x_1, \ldots, x_n)$ is called an R-function if it's sign is completely determined by the signs (but not magnitudes) of its arguments. A more general definition of R-mappings can be found in (Rvachev, 1967, 1982). Below we will use the following R-functions:

R – conjunction:

$$x \wedge_\alpha y = \frac{1}{1+\alpha}\left(x + y - \sqrt{x^2 + y^2 - 2\alpha xy}\right) \quad (1)$$

R – disjunction:

$$x \vee_\alpha y = \frac{1}{1+\alpha}\left(x + y + \sqrt{x^2 + y^2 - 2\alpha xy}\right) \quad (2)$$

where $-1 < \alpha \le 1$. In particular, for $\alpha = 1$, we have

$$x \wedge_1 y = \tfrac{1}{2}(x + y - |x - y|) = \min(x, y) \quad (3)$$

$$x \vee_1 y = \tfrac{1}{2}(x + y + |x - y|) = \max(x, y) \quad (4)$$

For $\alpha = 0$, we get one of the simplest and most widely used systems of R-functions:

$$x \wedge_0 y = x + y - \sqrt{x^2 + y^2} \quad (5)$$

$$x \vee_0 y = x + y + \sqrt{x^2 + y^2} \quad (6)$$

The above R-functions correspond to the Boolean logic functions $\wedge$ and $\vee$ in a precise sense which is explained below. We will also find useful the R-operation corresponding to logical equivalence $\sim$:

$$x \sim_n y = xy(x^n + y^n)^{-1/n}. \quad (7)$$

For positive x and y, this operation coincides with one of the operations discovered and used by Ricci (1973). A significant advantage of R-equivalence $\sim_n$ is its associativity:

$$\begin{aligned}(x \sim_n y) \sim_n z &= xyz(x^n + y^n)^{-1/n}(x^n y^n (x^n + y^n)^{-1} + z^n)^{-1/n} \\ &= xyz(x^n y^n + x^n z^n + y^n z^n)^{-1/n} \\ &= x \sim_n (y \sim_n z) = x \sim_n y \sim_n z.\end{aligned}$$

It is easy to see that R-operations $\wedge_1$ and $\vee_1$ are also associative. However, operations $\wedge_0$ and $\vee_0$ are not associative.

R-functions allow constructing normalized implicit functions for complex geometric objects. Let geometric domain $\Omega = F(\Sigma_1, \ldots, \Sigma_n)$ be constructed as a Boolean (union and intersection) combination of primitive regions Σ_i, with every Σ_i defined by a real-valued function inequality $(\sigma_i > 0)$. If f is an R-function of n arguments corresponding to the Boolean function F, then the implicit function for the resulting geometric domain is immediately given by $\Omega = (f(\sigma_1, \ldots, \sigma_n) > 0)$. Outside of Ω function $f(\sigma_1, \ldots, \sigma_n)$ is negative and the equation $f(\sigma_1, \ldots, \sigma_n) = 0$ defines the boundary Γ of the region Ω. Furthermore, if every primitive implicit function σ_i is normalized at the primitive boundaries, then all of the R-functions above preserve this property, and the function $f(\sigma_1, \ldots, \sigma_n)$ is normalized at the boundary Γ (Rvachev 1982). Construction of normal implicit functions is more difficult in general, but has been solved in many common situations described below.

2.2 Normal and Normalized Functions. Normal functions are known for many common geometric objects, for example:

- a line: $|x \cos\alpha + y \sin\alpha - p| = 0$;
- a circle: $|\sqrt{(x-a)^2 + (y-b)^2} - R| = 0$;
- a point: $\sqrt{(x-a)^2 + (y-b)^2} = 0$;
- an ellipse: $(ya^2 - \lambda x b^2/a^2 - b^2) - \sqrt{(1/\lambda^2) + 1} = 0$, where $\lambda(x, y)$ is the real root of equation

$$(\lambda x - y)^2(a^2 + \lambda^2 b^2) - \lambda^2(a^2 - b^2)^2 = 0,$$

which is related to the minimum value of normal function $\rho(x, y)$.

The normal function of a line segment is basically a Euclidean distance function; it is often constructed in a piecewise fashion by considering a Voronoi diagram for a line segment and its endpoints as shown in Fig. 1(a). But the normal equation of

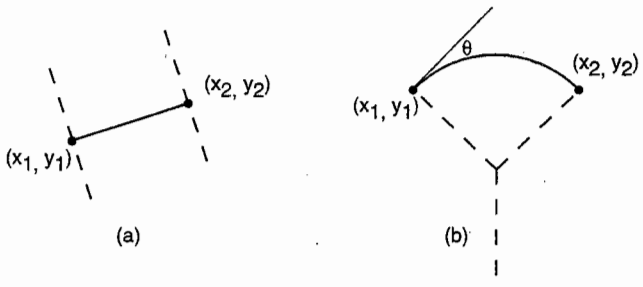

Fig. 1 Constructing normal (distance) functions for linear and circular segments.

the line segment with the endpoints at (x_1, y_1) and (x_2, y_2) can also be written explicitly as:

$$\varphi(x, y, x_1, y_1, x_2, y_2) \equiv \frac{1}{2}\left\{ - \frac{(f_1 - f_2)^2}{l^2} + \frac{(l^2 - f_3)^2}{2l^2}\left[1 - \text{sign}\left(1 - \frac{f_3^2}{l^4}\right)\right]\right\}^{1/2}, \quad (8)$$

where

$$f_1 = (2x - x_1 - x_2)(y_2 - y_1);$$
$$f_2 = (2y - y_1 - y_2)(x_2 - x_1);$$
$$f_3 = |(2x - x_1 - x_2)(x_2 - x_1) + (2y - y_1 - y_2)(y_2 - y_1)|;$$
$$l = \sqrt{(x_2 - x_1)^2 + (y_2 - y_1)^2}.$$

Similarly, the normal function for a circular arc can be constructed as shown in Fig. 1(*b*). If $M_1(x_1, y_1)$ and $M_2(x_2, y_2)$ are the beginning and the ending points respectively, then angle θ between the tangent at M_1 and the chord M_1M_2 is considered positive when the portion of a circle lies to the left of the vector $\overrightarrow{M_1M_2}$. Once again the normal equation can be written explicitly as

$$\varphi(x, y, x_1, y_1, x_2, y_2, \theta) \equiv \eta(x', y') + \frac{\xi(x', y') - \eta(x', y')}{2}[1 - \text{sign}\,\zeta(x', y')], \quad (9)$$

where

$$x' = f_3/2l;$$
$$y' = (f_2 - f_1)/2l;$$
$$\xi = \sqrt{(|x| - l/2)^2 + y^2};$$
$$\eta = \left|\frac{l}{\sin\theta} - \frac{1}{2\sin\theta}\sqrt{4x^2\sin^2\theta + (2y\sin\theta + l\cos\theta)^2}\right|;$$
$$\zeta = y\sin\theta + \frac{l}{2}\cos\theta - |x|\cos\theta.$$

It was shown in Rvachev (1982) that when $\theta = 0$ the normal function of an arc transforms into a normal function of a chord. An important advantage of explicit representations over procedural definitions of normal functions is that the defined functions are differentiable almost everywhere (except at the points that are equidistant from several points on the segment in question). The differential properties of constructed functions play an important role in modeling of solidification processes.

Normal functions and equations may be difficult to construct for some objects (for example, exponential and logarithmic boundaries require solving transcendental equations). However, as was shown in Rvachev (1982), a normal equation can be approximated with arbitrary precision by a finite number of arcs and line segments for any boundary.

If $f_1(x, y)$ is a normal function of the boundary L_1, and $f_2(x, y)$ is a normal function of the boundary L_2, the function

$$\varphi(x, y) = f_1(x, y) \wedge_1 f_2(x, y) \quad (10)$$

is a normal function of the boundary L that is the union of boundaries L_1 and L_2. However such a normal function is a distance function and is therefore not differentiable at any point that is equidistant from two or more boundary points (i.e., precisely at the points lying on the boundaries of Voronoi regions). In terms of modeling temperature fields, these derivative discontinuities correspond to discontinuities in heat fluxes, which contradicts the physical principles and the fourth postulate in section 1.2. Therefore instead we propose to use a normalized function

$$\varphi(x, y) = f_1(x, y) \sim f_2(x, y) = \frac{f_1(x, y)f_2(x, y)}{f_1(x, y) + f_2(x, y)} \quad (11)$$

which is consistent with the fifth postulate and is differentiable everywhere. This function corresponds to Boolean equivalence and is therefore called *R*-equivalence. Note that *R*-equivalence (11) approaches *R*-conjunction $f_1 \wedge_1 f_2$ for points that are close to the smooth parts of the boundary. In this case, if v is the *R*-conjunction of contributions from boundaries $L_1, L_2, \ldots, L_{i-1}, L_{i+1}, \ldots, L_n$ (but not L_i), and $u_i \ll v$, then

$$u = u_i \sim v = \frac{u_i v}{u_i + v} = \frac{u_i}{\frac{u_i}{v} + 1} = u_i \wedge_1 v + O\left(\frac{u_i}{v}\right).$$

In other words, $u \approx u_i$ near i-th region of the boundary. The situation changes in proximity to corner points. Near these points the normal functions of the sides of an angle are close in value, but small compared to normal functions of other sides. Thus the solution around a vertex formed by two edges with normal functions u_1 and u_2, will be approximately $u \approx u_1 \sim u_2$, which means that it will not be affected by other boundaries away from that vertex. It should be noted that the validity of operation $x \sim y$ is supported experimentally only in the vicinity of right angles. Other angles require modification of the construction procedure as we explain in section 3.1.

2.3 Modification of *R*-equivalence. One serious drawback of operation $x \sim y$ is that it grows unbounded (goes to infinity) as x and y go to infinity. Since x and y correspond to the respective distances from portions of the mold boundaries, such behavior contradicts the sixth postulate in section 1.2. One way to correct this undesirable effect is to directly modify *R*-equivalence as:

$$x \overset{\epsilon}{\sim} y = \frac{xy}{x + y + \epsilon xy}. \quad (12)$$

This new operation preserves most of the attractive properties of *R*-equivalence (summarized in the Appendix), including commutativity, associativity, and other convenient computational properties. We will also see in section 3.1 that parameter ϵ can be used to correlate the model with the known data about the ambient temperature at infinity.

3 Implicit Functions for Metal Solidification

3.1 Model Development. Modeling of the liquid metal solidification process in polygonal form castings was examined by Neises et al. (1987) and by Uicker and Sather (1992) using normal equations of boundaries and *R*-equivalence (9) to define the boundaries of the area under study and to visualize the temperature field distribution. One of the assumptions was steadiness of temperature at the border of the volume (assigned value zero for convenience). However, the possibility to provide various thermal fluxes through the faces (in 3D case) or edges (2D) was allowed. In this case, the normal functions of the edges u_i were used with the weight coefficients m_i that were inversely proportional to the gradients of the modeled field. Here we build on these earlier studies, and extend them including in terms of allowed heat exchange conditions with the environment and implementation of thermal interaction of two or more neighboring casts filled with metal within the same mold.

Due to the associativity of operation (11), we can include normal functions of the parts of the field boundary in an arbitrary order while constructing the function u of the temperature field. In this case, if the cast and the boundary conditions have the same type of symmetry, then this symmetry will be pre-

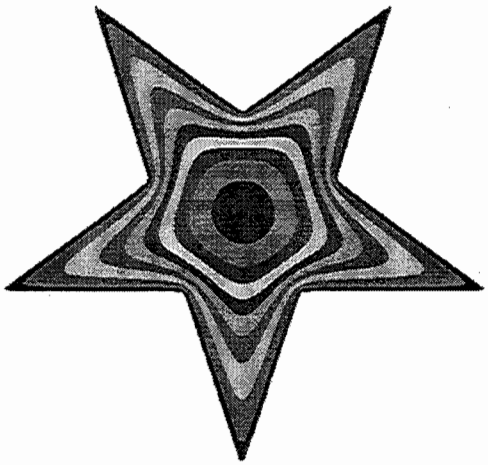

Fig. 2 Constructed implicit function preserves the symmetry

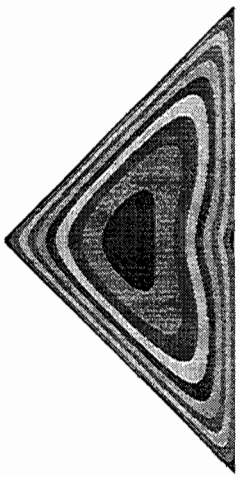

Fig. 4 Isolines of the implicit function are not consistent with physical postulates

served in the constructed implicit function (and the modeled temperature field). (See Fig. 2.)

In case of a right angle it was verified (Neises et al., 1987) that the actual temperature field is of the same type as the implicit function model defined by $(u_1/m_1) \sim (u_2/m_2)$, where u_1, u_2—normal functions of the two sides. However, it is not immediately clear whether the same procedure of building a function u as $u = (u_1/m_1) \sim (u_2/m_2) \sim \ldots (u_n/m_n)$ is applicable to other angles; and in fact it is easy to explain why it may inappropriate. To clarify this issue, a numerical experiment was conducted. The series of quadrangles with the vertices in A, B, C, D) was considered (refer to Fig. 3). When A coincides with point O the quadrangle degenerates into a triangle; when A coincides with point M the quadrangle is the square $ABCD$; the corresponding function can be written as

$$u = mm\left(\frac{u_{AB}}{m_{AB}} \sim \frac{u_{AD}}{m_{AD}} \sim \frac{u_{BC}}{m_{BC}} \sim \frac{u_{CD}}{m_{CD}}\right), \qquad (13)$$

where mm is some experimentally chosen scaling coefficient (as discussed below), and $m_{AB} = m_{AD} = m_{BC} = m_{CD} = 1$. Suppose that the equivalence operation can be applied also in the case of other positions of A (i.e. for other values of angle BAD). In particular, let us assume A is collinear with B and D (the angle BAD is 180 deg). According to the first postulate in section 1.2, the level lines of the modeled function u have to be straight along a straight border. As for isolines that are built according to formula (12), they actually have shapes as shown in Fig. 4 in this case. The contradiction with the assumption that the isolines near a straight border have to be parallel to the latter is apparent. To eliminate the found defect and in order to allow further correction of the behavior of u near a border vertex, it makes sense to use not only the normal equations for the smooth parts of the boundary, but also the normal functions of the vertices:

$$r_i = \sqrt{(x - x_i)^2 + (y - y_i)^2}$$

with corresponding coefficients k_i. Applying R-equivalence to all edges and vertices, equation (13) will assume the following form:

$$u = mm\left(u_{AB} \sim u_{AD} \sim u_{BC} \sim u_{CD} \sim \frac{r_A}{k_A} \sim \frac{r_B}{k_B} \sim \frac{r_D}{k_D} \sim \frac{r_C}{k_C}\right).$$

Along the radius OA $u_{AB} = u_{AD}$ and, according to property e),

$$u_{AB} \sim u_{AD} = \frac{u_{AB}}{2}.$$

Then

$$u = mm\left(\frac{u_{AB}}{2} \sim u_{BC} \sim u_{CD} \sim \frac{r_A}{k_A} \sim \frac{r_B}{k_B} \sim \frac{r_C}{k_C} \sim \frac{r_D}{k_D}\right),$$

and taking into account that along this radius $r_A = u_{AB}$, from $(u_{AB}/2) \sim (r_A/k_A) = u_{AB}$ we get $k_A = -1$ when $a = 0$. On the

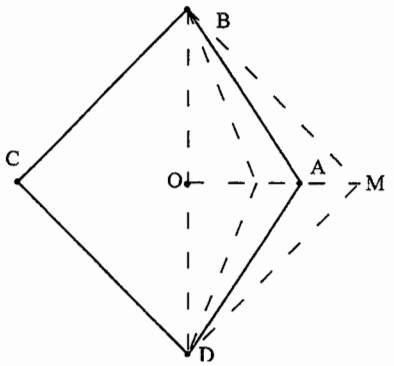

Fig. 3 A triangle shape as a limit of quadrilateral

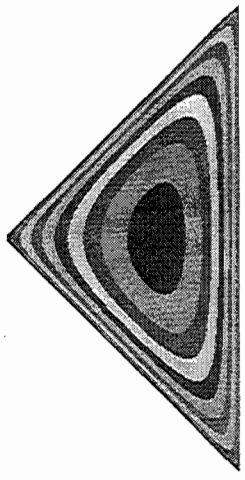

Fig. 5 Improved implicit function model using angle weights

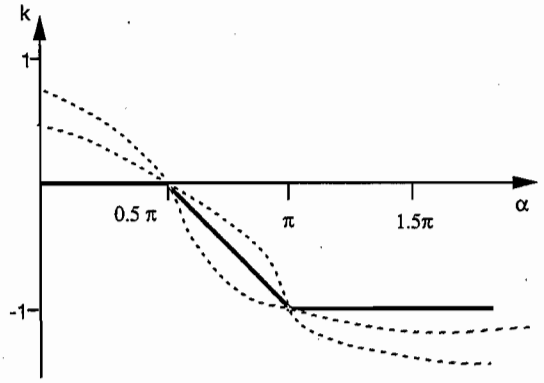

Fig. 6 Relationship between angle α and the weighting function $k(\alpha)$

other hand, when $a = 2$, i.e. in the case of a right angle, $k_A = 0$.

Thus, using the associativity of R-equivalence, the u function sought will be presented in form:

$$u = mm\left(\frac{u_1}{m_1} \sim \frac{u_2}{m_2} \sim \ldots \sim \frac{u_n}{m_n} \sim \frac{r_1}{k_1} \sim \frac{r_2}{k_2} \sim \ldots \sim \frac{r_n}{k_n}\right). \tag{14}$$

Note that if any of the k_i or m_i values approach zero, i.e. $(u_i/m_i) \to \infty (r_i/k_i \to \infty)$, then the corresponding component of Eq. (13) disappears, based on property (c) of R-equivalence in Appendix A. As shown in Fig. 5, the above approach eliminates the problems observed in Fig. 4, when the coefficients k_i vary from 0 to -1 as point A merges with point O. Hence, the dependence of coefficient k_i on the value of the angle has to be as is shown in Fig. 6. The values of function $k = k(\alpha)$ in points M and N are established and are reliable. The possible options of this dependence are shown in Fig. 6 as dotted lines. Numerical

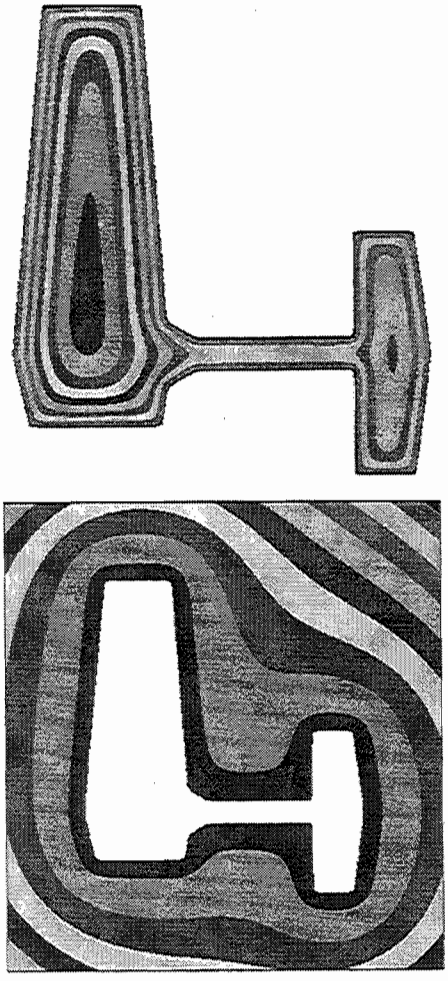

Fig. 7 Implicit function models for polygonal shapes

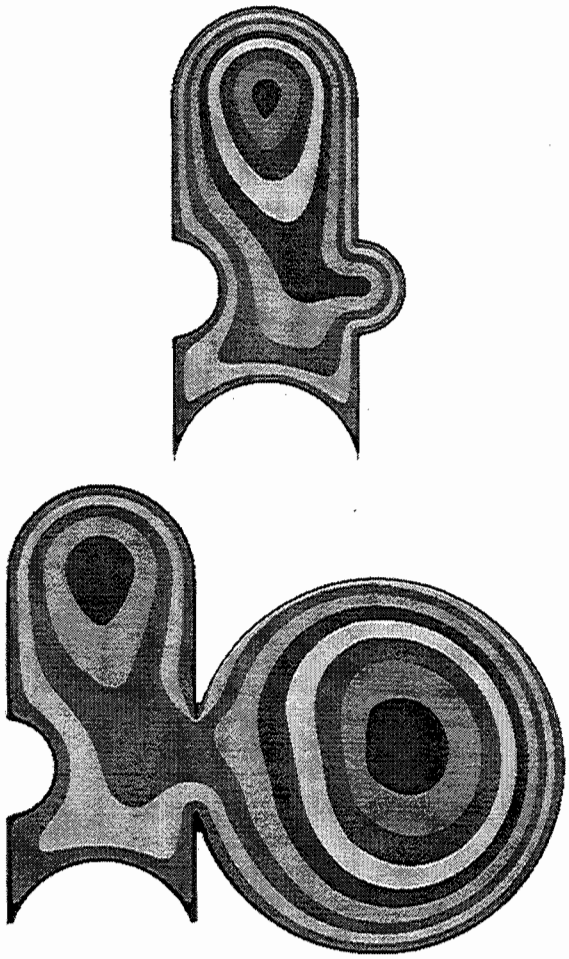

Fig. 8 Parametric studies of implicit function models

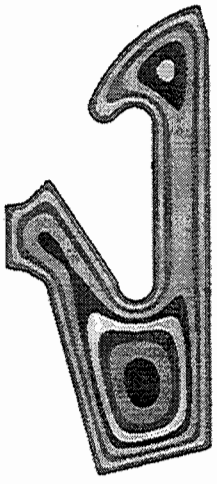

Fig. 9 A two-dimensional casting bounded by linear and circular segments

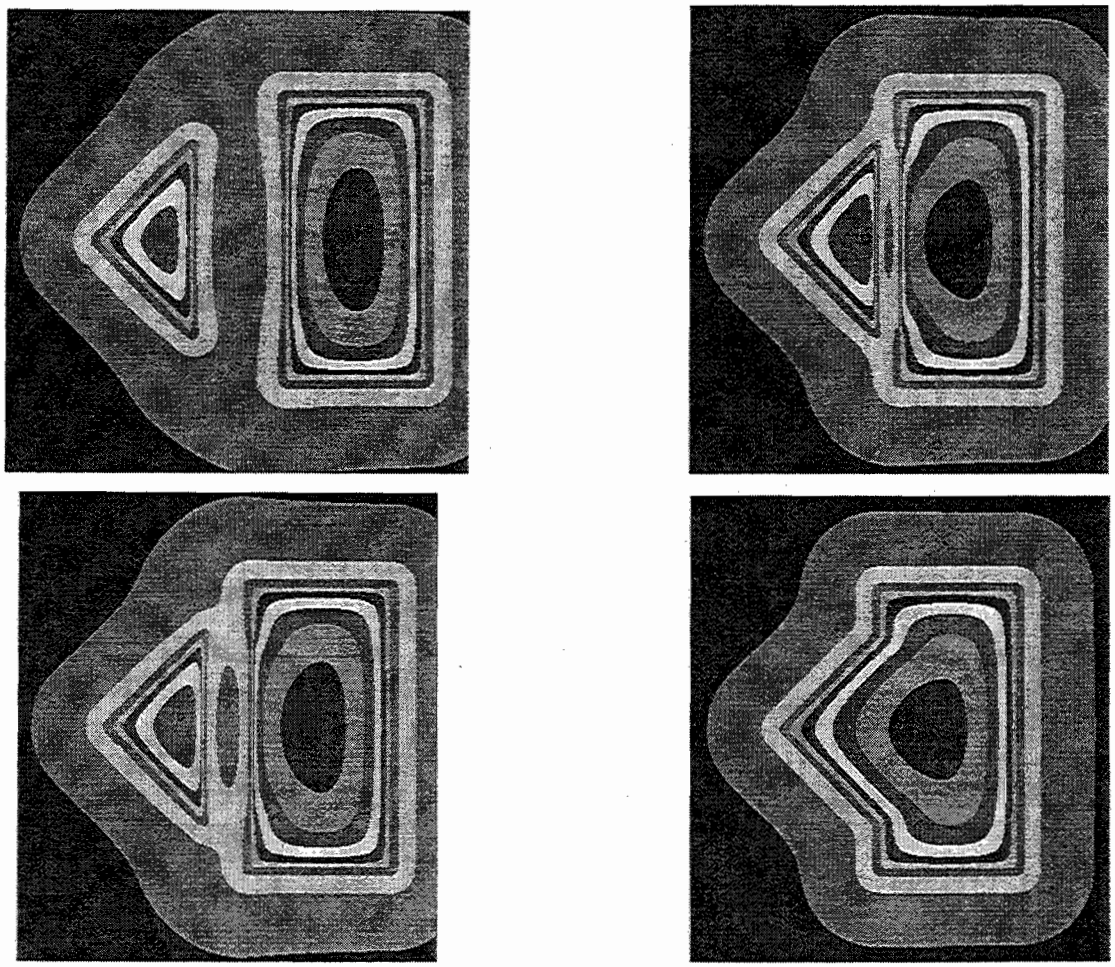

Fig. 10 Interacting fields of several castings

experiments showed that none of these choices lead to contradiction with the engineer's intuition about the character of a field around the vertex, so additional experimental data are necessary for getting the more precise correlation. For simplicity, we assume this dependence to be piecewise linear. This approach allows to formalize the process of choosing coefficients k_i and determine them from the geometrical characteristics of the cast cavity.

The choice of coefficient *mm* is based on experimental data and Chvorinov's rule (see section 1.2) and is proportional to ratio of area to perimeter in the case of a planar shape. This captures the relation between the temperature on the casting boundary and the maximum temperature of the liquid metal, as was originally suggested by Uicker and Sather (1992).

Finally, as we discussed in section 2.3, modification of *R*-equivalence using Eq. (12) does not undermine the validity of the above considerations. Accordingly, instead of the implicit function model of Eq. (14), we use a more practical expression:

$$u = \underset{\sim}{\overset{\epsilon}{}}_{i=1,n} \frac{u_i}{m_i} \underset{\sim}{\overset{\epsilon}{}}_{i=1,n} \frac{r_i}{k_i}, \tag{15}$$

where the choice of technological parameter ϵ is based on data about the ambient temperature at infinity.

If the computed temperature field is not satisfactory, it can be easily changed by manipulating parameters m_i that correspond to the temperature fluxes at the boundary. In particular, according to the third postulate, the undesirable local maxima can be shifted towards the boundaries for the purpose of elimination of defects in solidifying metal.

3.2 Implementation and Examples. The described techniques were fully implemented in a POLYE modeling system (Rvachev and Shevchenko, 1988) as a program that requires minimal input information about the form under study. Specifically, two-dimensional boundaries are described by a list of ordered line segments (specified by the coordinates of their end points) and circular arcs (described by the end points, center coordinates, and radii). Figures 7–10 show examples of the problems modeled and solved using the approach described in this paper.

- Figure 7 shows examples of computed temperature fields in polygonal castings. These examples were used as test runs in comparing the computed results with similar results reported in reference (Uicker and Sather, 1992).
- Castings bounded by arcs and line segments are shown in Figs. 8 and 9. The example in Fig. 8 illustrates parametric studies carried out in system POLYE. Changes of parameters of the circle are automatically propagated to implicit functions and the computed field, without any additional programming or constructions. The ease of such parametric studies is one of the advantages offered by *R*-function technology (Rvachev and Shevchenko, 1988).
- Figure 10 shows examples of several interacting fields of two or more castings. As in the case of simply connected domains, the governing assumption was that the field distribution was equidistant in nature, but was limited by the ambient temperature level (ϵ). In case of several interacting casting cavities, the already mentioned k_i parameter depends not only on the value of an angle at the vertex, but also on the relative position of the cavities: $k_i(\kappa) =$

$k_i(0) + \kappa(k_i(1) - k_i(0))$, where κ changes from 1 to 0. The same formula was used to find also parameter m_i. Figure 9*b* shows the results of merging two parts, where changes in corresponding parameters k_i and m_i take place.

The examples in Figs. 7–9 are intentionally very simplified and were chosen to enhance understanding of the methods involved. However, such simple example do not emphasize another primary advantage of the implicit function method, the speed advantage. The execution speed of analysis is improved by at least an order of magnitude over finite element or finite difference methods (Uicker and Sather, 1992). In addition, there is an even larger saving in model preparation time since no mesh is required. Also, for the same reason, accuracy cannot be degraded by an inappropriate mesh and no time is spent in iterating to improve the mesh.

4 Conclusions

4.1 Extensions to Three Dimensions. The described methods of modeling generalize to fully three-dimensional shapes. In particular, the required implicit functions can be automatically constructed for all solid objects (Shapiro, 1994), and the constructive techniques using *R*-functions remain identical. Normalized equations of line and circular segments become normalized equations of planar and quadratic surfaces and other three-dimensional primitives. Role of corner points in Eq. (14) will be played by the (possibly curved) edges of the solid, and the quantities r_i may become variable functions. Additional controlling component constants must be associated with each vertex of the solid (intersection of three or more faces). A number of methods for constructing the required functions associated with faces, edges, and vertices of solids based on the theory of *R*-functions are known (Rvachev, 1982). As in the two-dimensional case, the qualities of the resulting temperature field and the interface between liquid and solid metal may be characterized by the isothermal surfaces, which could be visualized in plane sections of the solid.

4.2 Methodology of Implicit Functions. In addition to metal solidification modeling, the mathematical machinery developed in this work is applicable to many other applications where the physical process can be described through an evolution of a geometric form, based on experimental data and/or engineering intuition. For instance, predicting the depth of penetration of a given heat treatment process on hardness in the interior of a heat treated metal part can be found directly from the normalized functions discussed in this paper. The only extension required is that a standard "Jominy bar" test be used for the given heating process to calibrate the iso-function values with measured metal hardness values.

In many realistic situations, the physical phenomena are so complex that constructing and investigating their integral-differential mathematical models may not be practical. In such situations, a simpler empirical approach, such as our approach to solidification, may also provide a reasonable alternative for predicting engineering analysis results with sufficient confidence level. For example, the spread of forest or prairie fires may be determined by a large number of factors: combustion rates, wind direction, natural water barriers, and so—all of which may be measured with reasonable precision. The initial shape of the fire may significantly influence the evolution of the front. Other problems that possess similar characteristics include corrosion processes (even if much slower than the fire problem described above) and the solid rocket fuel combustion. It will be also interesting to see if the proposed methodology may be used in design and fabrication of microelectromechanical systems (Kota et al., 1994), where the characteristics of the etched shapes are often predicted by evolving geometric boundaries (Hubbard and Antonsson, 1994).

5 Acknowledgments

This work was supported in part by NATO grant HTECH.LG 941352 and National Science Foundation grant DMII-9522806; in addition, V. Shapiro is supported by the National Science Foundation CAREER award DMII-9502728, and V. L. Rvachev by the International Soros Science Education Program of International Research Foundation grant SPU 071055.

References

1 Chvorinov, N., "Theory of Solidification of Casting," *Die Giesserei.* Vol. 27, May 17 to June 14, 1940, pp. 17–224.

2 Hubbard, T. J., and Antonsson, E. K., "Emergent Faces in Crystal Etching," *Journal of Microelectromechanical Systems,* Vol. 3, No. 1, March 1994, pp. 19–27.

3 Kota, S., Ananthasuresh, G. K., Crary, S. B., and Wise, K. D., "Design and Fabrication of Microelectromechanical Systems," ASME JOURNAL OF MECHANICAL DESIGN, Vol. 116, December 1994, pp. 1081–1087.

4 Kutsenko, L. H., *Computer Graphics in Design Problems,* Series "Mathematics and Cybernetics," No. 8. Znaniye, Moscow, 1990, In Russian.

5 Kutsenko, L. H., and Markin, L. V., *Shapes and Formulas,* MAI Publisher, Moscow, 1994, In Russian.

6 Mikhailov, A. M., Bauman, B. V., and Blagov, B. N., *Metal Casting Manufacturing,* Machinostroyenie, Moscow, 1987, In Russian.

7 Neises, S. J., Uicker, J. J., Jr., and Heine, R. W., "Geometric Modeling of Directional Solidification Based on Section Modulus," *AFS Transactions,* Vol. 95, 1987.

8 Ricci, A., "A Constructive Geometry for Computer Graphics," *Computer Journal,* Vol. 16, No. 3, May 1973, pp. 157–160.

9 Rvachev, V. L., *Theory of R-functions and Some Applications,* Naukova Dumka, Kiev, 1982, In Russian.

10 Rvachev, V. L., *Geometric Applications of Logic Algebra,* Naukova Dumka, Kiev, 1967, In Russian.

11 Rvachev, V. L., and Sheiko, T. I., "*R*-functions in Boundary Value Problems in Mechanics," ASME *Applied Mechanics Reviews,* Vol. 48, No. 4, April 1995.

12 Rvachev, V. L., and Shevchenko, A. N., *Problem-oriented Languages and Systems for Engineering Computations,* Teknika, Kiev, 1988, In Russian.

13 Shapiro, V., *Theory of R-functions and Applications: A Primer,* Tech. Report CPA88-3 Cornell Programmable Automation, Cornell University, Ithaca, NY, November 1988.

14 Shapiro, V., "Real Functions for Representation of Rigid Solids," *Computer Aided Geometric Design,* Vol. 11, 1994, pp. 153–175.

15 Uicker, J. J. Jr., and Sather, L. E., "SWIFT: A Modulus Approach to the Simulation of the Casting Process," *Ductile Iron Solidification Modeling,* Vol. 176, 1992.

APPENDIX

Formal Properties of Modified *R*-Equivalence

(a) Commutativity $x \overset{\epsilon}{\sim} y = y \overset{\epsilon}{\sim} x$;
(b) Associativity

$$(x \overset{\epsilon_i}{\sim} y) \overset{\epsilon_j}{\sim} z = x \overset{\epsilon_i}{\sim} (y \overset{\epsilon_j}{\sim} z) = x \overset{\epsilon_j}{\sim} (y \overset{\epsilon_i}{\sim} z)$$
$$= x \sim (y \overset{\epsilon_i+\epsilon_j}{\sim} z) = x \overset{\epsilon}{\sim} y \overset{\epsilon}{\sim} z,$$

where $\epsilon = (\epsilon_i + \epsilon_j)/2$. Indeed,

$$(x \overset{\epsilon_i}{\sim} y) \overset{\epsilon_j}{\sim} z = \frac{\dfrac{xy}{x + y + \epsilon_i xy} z}{\dfrac{xy}{x + y + \epsilon_i xy} + z + \dfrac{xyz\epsilon_j}{x + y + z + \epsilon_i xy}}$$

$$= = \frac{xyz}{xy + yz + xz + (\epsilon_i + \epsilon_j)xyz}$$

$$= x \overset{\epsilon_i}{\sim} (y \overset{\epsilon_i}{\sim} z) = x \overset{\epsilon_j}{\sim} (y \overset{\epsilon_i}{\sim} z)$$

$$= x \sim (y \overset{\epsilon_i+\epsilon_j}{\sim} z) = x \overset{\epsilon}{\sim} y \overset{\epsilon}{\sim} z;$$

(c) Limiting properties

$$\lim_{y \to \infty} x \overset{0}{\sim} y = x;$$

$$\lim_{x_1 \to \infty} \overset{\epsilon_i}{\sim}_{i=1,n} x_i = \overset{\epsilon_i}{\sim}_{i=2,n} x_i;$$

(e) Averaging of equal elements $x \sim x = (x/2)$;

(k) Elimination of opposite elements $\lim_{z \to -y} (x \sim y \sim z) = x$;

(l) $\overset{\epsilon_i}{\sim}_{i=1,n} x_i = [\sum_{i=1}^{n} (x_i)^{-1} + \sum_{i=1}^{n} \epsilon_i]^{-1}$;

(m) $\overset{\epsilon_i}{\sim}_{i=1,n} x_i = \overset{\epsilon}{\sim}_{i=1,n} x_i$, where $\epsilon = (\sum_{i=1}^{n} \epsilon_i)/(n-1)$.

The last two properties further simplify computations involved in applying the operation to n arguments and are convenient for algorithm development.